Available online at www.sciencedirect.com
ScienceDirect
Catalysis Today 122 (2007) 101–108
CATALYSIS TODAY
www.elsevier.com/locate/cattod

Temperature dependent photoluminescence of photocatalytically active titania nanopowders

Herrade Bieber [a,b], Pierre Gilliot [a], Mathieu Gallart [a], Nicolas Keller [b], Valérie Keller [b], Sylvie Bégin-Colin [a,*], Catherine Pighini [c], Nadine Millot [c]

[a] *Institut de Physique et Chimie des Matériaux, UMR CNRS-ULP-7504, 23 rue du Loess, 67034 Strasbourg Cedex, France*
[b] *Laboratoire des Matériaux, Surfaces et Procédés Pour la Catalyse, UMR 7515 CNRS and ELCASS (European Laboratory for Catalysis and Surface Sciences), Louis Pasteur University, 25 rue Becquerel, 67087 Strasbourg Cedex, France*
[c] *Laboratoire de Recherche sur la Réactivité des Solides, UMR 5613 CNRS/Université de Bourgogne, BP 47 870, 21078 Dijon Cedex, France*

Available online 1 February 2007

Abstract

Temperature photoluminescence (PL) in the sub-ambient range has been developed as a tool for characterizing photocatalytic materials. The use of well-characterized TiO_2 nanoparticles with calibrated particle sizes allowed to face the temperature dependent PL results with the photocatalytic activity and several important physico-chemical parameters. In the relaxation of the photoexcited electron/hole pairs, the transfer towards surface sites is in competition with radiative and non-radiative recombinations. Temperature dependent PL appears thus to be a very sensitive technique to study the efficiency of the electron or the hole trapping at the surface of titania nanoparticles where they take part to the oxidation/reduction reactions. The PL shows a peak around 610 nm with a width of about 130 nm. The quenching of this emission is measured as a function of the temperature, from 9.9 up to 230 K. The kinetics of this phenomenon can be described by fitting the temperature dependent PL results with a double activation law while a simple activation model fails. It suggests that two ways are involved in the trapping process of the carriers, with activation energies in the range of a few meV and a few tenths of meV, respectively. The relationship between the PL parameters linked to the two different energetic processes associated to two energy barriers (activation energy and transition rate), the powder characteristics and the photoactivity is discussed.

Keywords: TiO_2 nanoparticles; Charge recombination; Temperature dependent photoluminescence

1. Introduction

Heterogeneous photocatalysis has received increasing interest since the last decades for gas/liquid phase and surface applications in various fields, such as contaminated water and wastewater treatments, contaminated air clean up processes, renewable energy source production, self-cleaning materials or surface hydrophilicity/hydrophobicity properties [1]. In parallel to adsorption–desorption problems of both reactants and reaction products, the main limitation of the photocatalyst performances results from the recombination of photogenerated electron–hole pairs, which strongly reduces the density of photogenerated charge carriers at the active particle surface, available for initiating redox reactions with adsorbed surface species. Amongst several interesting ways, the coupling of different semiconductor phases, in which many research groups are involved, is a promising alternative to achieve an improved and efficient charge separation, and thus high photocatalytic performances in both gas and liquid applications [2–5].

Amongst different techniques used in photophysic and photocatalysis, photoluminescence characterization is an effective way to investigate the electronic structure and the optical characteristics of semiconductor nanomaterials, by which information, such as the separation and the recombination of photoinduced charge carriers as well as the surface oxygen vacancies and the defects can be obtained [6–8]. An extensive and fundamental detailed review has been published by Anpo and Che [9]. Therefore, photoluminescence is usually reported as a highly significant and informative characterization method for preparing high activity photocatalysts.

* Corresponding author. Tel.: +33 388107247; fax: +33 388107192.
E-mail address: sylvie.begin@ipcms.u-strasbg.fr (S. Bégin-Colin).

0920-5861/$ – see front matter © 2007 Elsevier B.V. All rights reserved.
doi:10.1016/j.cattod.2007.01.036

Photoluminescence spectra were generally obtained at room temperature and at 77 K to study the electron–hole recombination, correlation being observed between the photocatalytic activity and the photoluminescence spectrum results [7].

The oxidative photocatalytic removal of the gaseous methylethylketone volatile organic compound (MEK) has been chosen as a test reaction, studied in the laboratory [5]. Studying the degradation of this molecule remains nevertheless of high environmental and practical interest, since the almanac published by Cleming reports that, together with methanol, toluene, acetone, methylchloroform, xylenes and methylchloride, MEK belongs to the top 10 US toxic chemicals released in the atmosphere in 1991 [10].

Compared to works reporting photoluminesence at 77 K or room temperature on photocatalysts, such as TiO_2, the aim of this article is to report on the use of temperature photoluminescence from 9.9 to 230 K, performed on well-characterized and calibrated TiO_2 nanopowders. This allowed two different energetic processes to be clearly evidenced.

2. Experimental

2.1. TiO_2 synthesis

TiO_2 powder was synthesized by a sol–gel procedure in which hydrolysis occurs by adding 80 ml of distillated water to 37,5 g of $Ti[OCH(CH_3)_2]_4$ titanium tetra-isopropoxide (TTIP, Fluka, purum) dissolved in 80 ml of ethanol. The pH was maintained at 9 by dropwise addition of an ammonia aqueous solution (30% volume). After evaporation of the solvent, washing and drying overnight at room temperature and further at 110 °C, the resulting $Ti(OH)_4$ hydroxide amorphous powder has been calcinated at 420 °C for 5 h.

Two TiO_2 nanopowders, labeled HT1 and HT2, have been obtained by continuous hydrothermal synthesis in subcritical water from bis(ammonium lactato)titanium dihydroxide (ALT, Aldrich). The experimental apparatus used for the hydrothermal synthesis is described in Ref. [11]. The metal salt aqueous solution was prepared and fed into the apparatus in one stream, while in another stream, distilled water was pressurized and heated to a temperature above the desired temperature. The pressurized metal salt solution stream and the pure subcritical water stream were combined in a mixing zone just before the reactor, which led to rapid heating and subsequent reaction in the reactor. The residence time of the solution in the reactor was around 10 s. HT1 and HT2 TiO_2 nanopowders have been synthesized at 350 °C and 200 bar, and at 300 °C and 300 bar, respectively. After the reactor, the solution was rapidly quenched and filters removed agglomerated particles. Both powders in the resulting suspension have been centrifuged, washed several times with deionized water under sonication for 5 min and freeze-dried. More details on the continuous hydrothermal synthesis of nanostructured inorganic powders under subcritical or supercritical conditions can be found in Refs. [12,13].

TiO_2 P25 (Degussa, 50 m^2/g, anatase/rutile ratio of 80/20) has been used as reference, as usually for the photocatalytic degradation of the organic pollutants in water and air.

2.2. Characterization techniques

Structural characterization of the samples was done by powder XRD measurements, carried out with a Siemens Diffractometer Model D-5000, using a Cu Kα radiation and operating at 40 kV and 20 mA. The measurements were made using slow scan (10 s) and small step (0.02° 2θ) conditions. The mean crystallite size, i.e. the average size of the coherently diffracting domains, was determined from the Scherrer equation with the normal assumption of spherical crystallites:

$$D_c = \frac{K\lambda}{b_{hkl}}\cos\theta$$

where D_c (nm) is the average particle size, K the constant of diffraction taken to be unity, λ (nm) the X-ray wavelength, and b_{hkl} being the peak width at half-maximum for the hkl peak, corrected from instrument broadening and broadening due to the $K\alpha_2$ radiation. The anatase and rutile TiO_2 phases were evidenced according to the JCPDS files no. 21-1275 and 21-1276, respectively.

The surface area measurements were performed on Coulter SA-3100 and Belsorp-mini porosimeters using N_2 as adsorbent at LN_2 temperature. Before each measurement, the sample was evacuated for several hours in order to desorb the impurities adsorbed on its surface. Surface areas were calculated from the N_2 adsorption isotherms using the BET method and the microporous contents were derived from the well-known t-plot method. The theoretical grain size d was deduced from the $S_{BET} = 6/d\rho$ equation according to the usual spherical particle assumption, with a ρ mass density at 3.88 g/cm^3. The size and the size-distribution of HT1 and HT2 powders have been determined in Ref. [13] thanks to low frequency Raman scattering. The size determined by this method is in agreement with the size obtained by the other methods.

X-ray photoelectron spectroscopy (XPS) surface characterisation was performed using an aluminium anode energy source at Kα = 1486.6 eV. All the spectra were decomposed assuming several contributions, each of them having a Doniach and Sunjic shape [14] and a Shirley background subtraction [15].

High-resolution TEM characterization was performed using a 2010 FEG-TEM operating at 200 kV for high-resolution imaging with a practical resolution of 0.19 nm. TEM images were recorded with a TOPCON model 002B transmission electron microscope, operating at 200 kV, with a point to point resolution of 0.18 nm.

2.3. Photocatalytic device for MEK oxidation and procedure

The photocatalytic oxidation of MEK was carried out in a 300 mm length cylindrical concentric tubular Pyrex reactor made of two coaxial tubes 4 mm apart, between which the reactant mixture was passing through. Details concerning both reactor and device can be found in Ref. [16]. The 440 mg of TiO_2 photocatalyst were evenly coated on the internal surface of the external tube, diameter 35 mm, by evaporating a TiO_2-containing aqueous slurry to dryness. The coated reactor was

dried at 110 °C for 1 h in air. MEK (Fluka, >99.5%) and water were fed at ambient temperature and atmospheric pressure by bubbling air through two saturators, respectively, and mixed with additional air (Tylan MFC 260 mass-flow controllers) to obtain the required MEK–water–air ratios with a constant total air flow of 200 cm^3/min. The MEK content was set at 1500 vppm. The relative humidity was set at 50, 100 vol.% of relative humidity being defined as the saturated vapor pressure of water at 25 °C, which corresponds to about 24 Torr, i.e. about 3 vol.% relatively to the total atmospheric pressure. Before the photocatalytic reaction, the catalyst was first exposed to the polluted air stream with no illumination until dark-adsorption equilibrium is reached. Afterwards the UV illumination was switched on. Illumination was provided by a commercially available 8 W black light tube with a spectral peak centered around 380 nm, located inside the inner tube of the reactor. The reaction products were analyzed on-line by a thermal conductivity detector on a micro-gas chromatography (HP microCG M200H) allowing detection and quantification of MEK, water, CO_2 and organic by-products on OV1 and Poraplot Q columns.

2.4. Temperature dependent photoluminescence

The temperature dependent photoluminescence (TPL) experiments have been performed at different sub-ambient temperatures, from 5 up to 230 K, on an Oxford MG11 device in which the sample was surrounded by cold gaseous helium. The temperature of the sample was thus precisely monitored and controlled, and any surface heating resulting from the optical excitation was immediately dissipated. Tuning the helium flow issued from the helium tank and varying the heating obtained by an electrical resistance allowed a perfect control of the helium temperature and consequently of the sample to be obtained, from 4 K (the liquid helium temperature) to room temperature. The surrounding helium gas prevents the crystallites to be in contact with oxygen but it does not prevent the presence of adsorbed oxygen and physisorbed water at the surface of the nanoparticles. This allows to use our results to understand the behavior of the titania particles in air. Jung et al. have reported that larger quenching in the photoluminescence intensity means larger amounts of surface-active sites easily reacting with the oxygen [7]. The low temperatures and the use of helium in the present study did not allow to evidence such a phenomena.

The exciting light, provided by a 1 kW HBO mercury lamp, was spectrally filtered by a UG11 colored glass filter (Schott) which removes all the visible light emitted by the lamp above 400 nm, before being focused onto the samples. UV lines of the mercury emission are thus selected around 365 and 300 nm, with wavelengths below the absorption edge of the TiO_2 particles. The PL spectra show, as usual, a large Stokes shift with respect to this absorption.

The TiO_2 materials have been crushed and further pressed into pellets which have been fastened on the sample holder of the cryostat. The PL emission was collected by two lenses, taking care to reject the light which was reflected by the sample and to remove scattered light with a low-pass glass filter. The light was then focused onto the input slit of a 27-cm spectrometer and detected by a cooled CCD.

3. Results and discussion

3.1. Material characterization

Fig. 1 displays the XRD patterns of P25 TiO_2, sol–gel TiO_2 powder and both HT1 and HT2 TiO_2 nanopowders. Except for the P25 TiO_2 sample, for which both anatase and rutile phases were indexed with the usual 80:20 atomic ratio, the X-ray diffraction peaks could be assigned to the pure anatase phase. The average crystallite size was estimated according to the Debye–Scherrer equation (Table 1). The diffraction peaks of HT nanopowders are very broad by comparison with those of sol–gel powders, suggesting a very small crystallite size, estimated at 5.6 and 3.7 nm for the HT1 and HT2 powders, respectively. HT1 and HT2 nanopowders have high specific surface areas of 240 and 308 m^2/g, respectively, with no micropore content, which confirmed the small particle size of the powders. Mean particle sizes calculated from BET measurements assuming a spherical shape of nanoparticles displayed a relatively good agreement with those deduced from XRD measurements, especially for HT nanopowders for which mean particle sizes of 6.4 and 5.0 nm are obtained. This observation was confirmed by HRTEM observations, which evidenced that HT nanopowders were nearly monodisperse (Fig. 2), by contrast to sol–gel powders which exhibited a slightly more heterogeneous particle size distribution (see Ref. [13] for a detailed study of the grain size distribution by Raman scattering of HT1 and HT2 powders).

XPS analysis is usually used to evaluate the valence state of titanium atoms and the evolution of hydroxyl groups at the TiO_2 surface [17–20]. Whatever the TiO_2 powders, the Ti 2p XPS spectra confirmed that Ti is in the +4 oxidation state at the surface. By contrast, the O 1s XPS spectra displayed two contributions corresponding to a titanium–oxygen binding, attributed

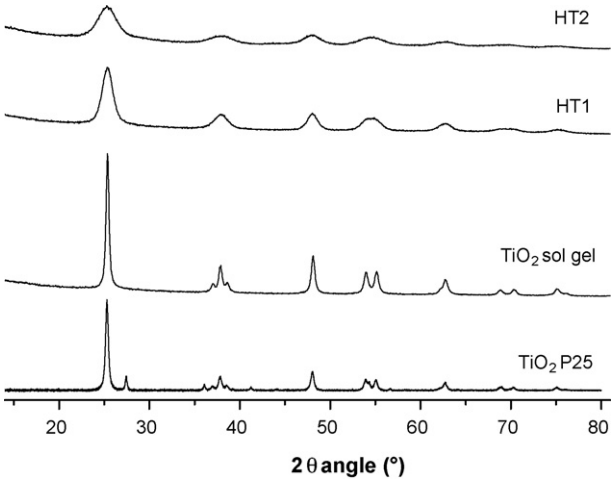

Fig. 1. XRD patterns of hydrothermally synthesized TiO_2 nanopowders (HT1 and HT2), TiO_2 sol–gel and commercially available TiO_2 P25.

Table 1
BET specific surface area with microporous content, average crystallite size from XRD results and average particle sizes deduced from BET measurements, O/Ti surface atomic ratio and OH content calculated from XPS measurements for the TiO_2 powders

	%Anatase	BET area [micropores] (m^2/g)	Average particle size from BET measurement (nm)	Average crystallite size from XRD results (nm)	O/Ti surface atomic ratio from XPS results	Content of OH (%) from XPS results
TiO_2 P25	80	50 [0]	31 ± 1	25 ± 1 (anatase)	2.2 ± 0.2	12
TiO_2 sol–gel	100	60 [0]	26 ± 1	22 ± 1	2.2 ± 0.2	23
TiO_2 HT1	100	240 [0]	6.4 ± 1	5.6 ± 1	2.2 ± 0.2	18
TiO_2 HT2	100	308 [0]	5.0 ± 1	3.7 ± 1	2.1 ± 0.2	30

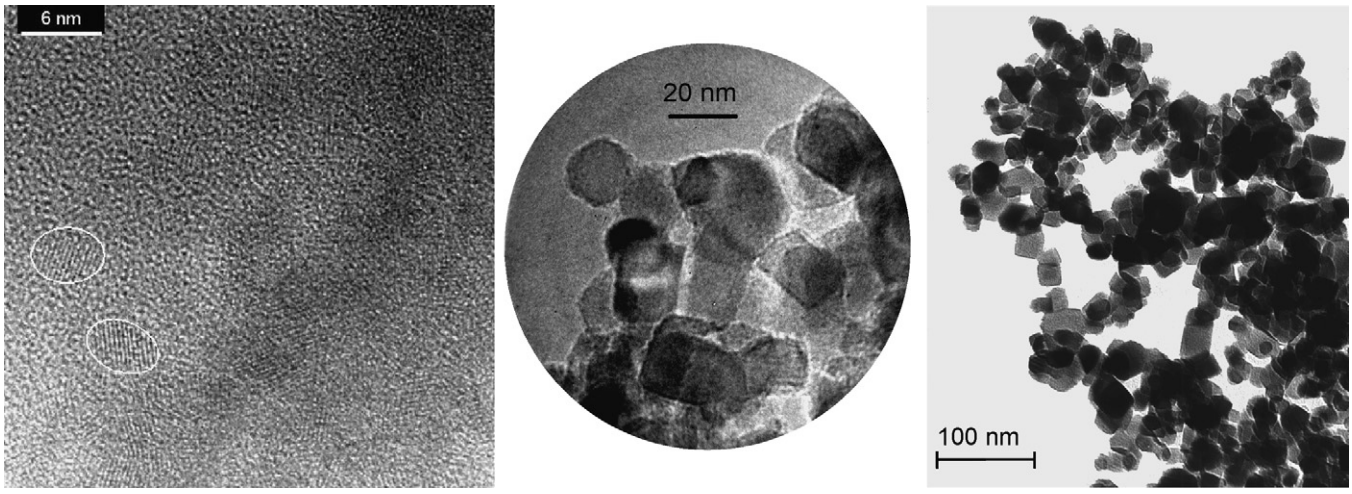

Fig. 2. HRTEM images of: (left) the HT2 TiO_2 nanopowder, (middle) the sol–gel TiO_2 and (right) the P25 TiO_2.

to Ti–O bonds in TiO_2 (network oxygen) and to the hydroxyl (Ti–OH) groups at the surface of TiO_2 powders, together with the high binding energy contribution assigned to the residual adsorbed water molecules (Fig. 3). Table 1 shows the OH surface content and the oxygen-to-titanium (O/Ti) surface atomic ratios calculated using the sensitivity factors and the transfer function of the spectrometer. Whatever the TiO_2 photocatalysts, the O/Ti surface atomic ratios were calculated at 2.1–2.2, while the OH surface contents were ranging from 12 to 30%.

The UV–vis absorbance spectra performed on the different TiO_2 photocatalysts did not show any significant differences and exhibited the usual absorption of anatase-based materials.

3.2. Photocatalytic and photoluminescence results

Tables 2 and 3 show the photocatalytic performances for the degradation of MEK in terms of MEK conversion, obtained over the different TiO_2 powder samples. The reported values are measured on stream at the steady-state under UV, after the dark-adsorption pretreatment initial period. The HT1 nanopowder (5.6–6.4 nm) and the P25 TiO_2 exhibited a high photocatalytic activity, at 96 and 89%, respectively, whereas an intermediate conversion of 55% was obtained over the HT2 nanopowder (3.7–5.0 nm) and a very low conversion of 24% was reached over the sol–gel TiO_2.

Typical PL spectra are presented in Fig. 4. The emission peak of P25 TiO_2 powders is centered on about 610 nm (2.030 eV) and covers a large part of the visible spectral range, with a width of about 130 nm (0.4 eV) taken as the full-width half-maximum (FWHM). The spectra are asymmetric, with a tail to low photon energies. It shows two bumps near the maximum. They could be related to two different contributions to the emission that have not been identified up to now. The peak position for each sample is given in Table 3.

Table 2
Adsorption capacities of the TiO_2 samples relatively to MEK (μmol/g) and H_2O (mmol) molecules during the on stream dark-pretreatment period

	S_{BET} (m^2/g)	Adsorbed MEK (μmol/g)	Adsorbed H_2O (mmol/g)	MEK adsorbed per meter square of TiO_2 surface (μmol/m^2)	Adsorbed H_2O per meter square of TiO_2 surface (mmol/m^2)	Conversion of MEK (%)
Sol–gel TiO_2	60 [0]	101	1.50	1.6	0.025	24
TiO_2 HT2	308 [0]	330	22.5	1.1	0.07	55
TiO_2 P25	50 [0]	112	0.63	2.2	0.01	89
TiO_2 HT1	240 [0]	275	17.6	1.2	0.07	96

They have been corrected from the surface area of TiO_2 available for the reactant adsorption, and thus expressed as μmol/m^2 and mmol/m^2, respectively.

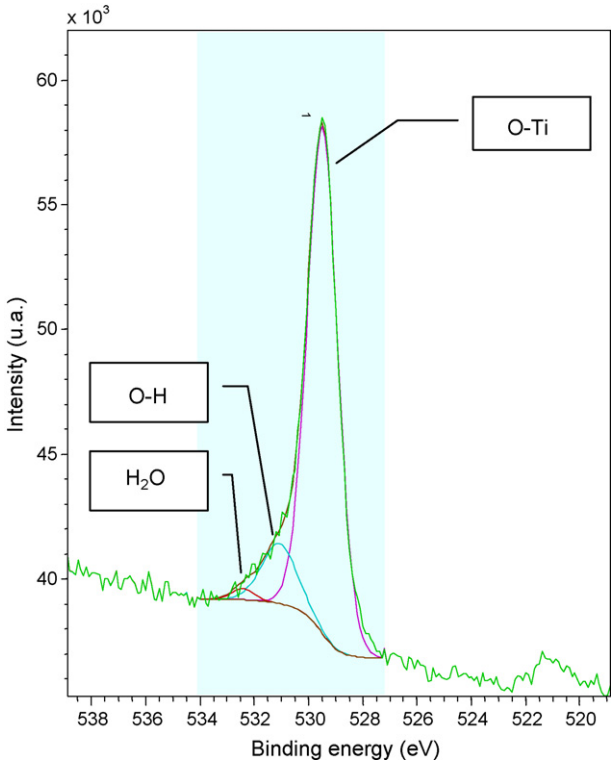

Fig. 3. XPS spectra of the O 1s region for the P25 TiO_2 photocatalyst. The subtraction of the energy shift due to electrostatic charging was determined using the contamination carbon C 1s band at 284.6 eV as reference.

As shown by Fig. 4, the PL intensity decreases when increasing the sample temperature. Fig. 5 plots the intensity of the emission, integrated over the full spectral range, as a function of the temperature. The decay with the temperature suggests a quenching of the luminescence which is thermally activated. The spectrally integrated PL intensity has been fitted as a function of the temperature by an activation law describing the transfer of photocarriers to non-radiative states. Let us consider a simple three level system, with E_0 being the ground state, E_1 (population n_1) the titania radiative state and E_a (population n_a) is a non-radiative surface state able to trap the photocarriers. Electron–hole pairs are generated at high photon energy in the bulk of the TiO_2 particles and then relax down to the level 1 (dotted lines in Fig. 6). The whole generation rate is denoted g. Two processes are further competing: whether the pairs recombine radiatively with a decay time τ_1, or they are trapped to the levels a and b. The rate equations for this model write:

$$\begin{cases} \dfrac{dn_1}{dt} = -\dfrac{n_1}{\tau_1} - \dfrac{n_1}{\tau_\uparrow} + \dfrac{n_a}{\tau_\downarrow} + g \\ \dfrac{dn_a}{dt} = -\dfrac{n_a}{\tau_a} - \dfrac{n_a}{\tau_\downarrow} + \dfrac{n_1}{\tau_\uparrow} \end{cases}$$

τ_1 and τ_a are the lifetime of levels 1 and a, respectively. Concerning the level 1, τ_1 is the radiative recombination time. $\tau_\uparrow$ and $\tau_\downarrow$ are the time constants relative to the escape from E_1 to E_a and to the back transfer from E_a to E_1, respectively. g is the generation rate. In the steady state regime, when the thermal equilibrium is reached, we can write:

$$\frac{n_1^{(0)}}{\tau_\uparrow} = \frac{n_a^{(0)}}{\tau_\downarrow}$$

which leads to:

$$\frac{\tau_\uparrow}{\tau_\downarrow} = \exp\left(\frac{\Delta E}{k_B T}\right)$$

where ΔE is the energy difference $E_a - E_1$.

For $T = 0$ K, $\tau_\uparrow$ tends towards $+\infty$ while $\tau_\downarrow$ tends towards a finite value labeled τ_0. Consequently, the radiative efficiency associated with the recombination from the level to the ground state can be expressed as:

$$\eta(T) = \frac{\tau_\uparrow}{\tau_\uparrow + \tau_1} = \frac{1}{1 + A\exp(-(\Delta E/k_B T))}$$

with $A = \tau_1/\tau_0$.

This time ratio corresponds also to the ratio of the probability, for the carriers, to be transferred to non-radiative states over the probability to recombine radiatively, in the limit of high temperatures. Moreover, if we assume η to be equal to 1 for very low temperatures the photoluminescence intensity, as a function of T, writes:

$$I(T) = \frac{I_0}{1 + A\exp(-(\Delta E/k_B T))}.$$

According to Fig. 5, it appeared that two-activation processes with different activation energies have to be considered in order to fit the experimental data. In this case, the above expression becomes the law:

$$I(T) = \frac{I_0}{1 + A_a\exp(-\Delta E_a/k_B T) + A_b\exp(-\Delta E_b/k_B T)}$$

T is the temperature, k_B the Boltzmann constant, I_0 the emission intensity in the limit of very low temperatures, ΔE_a and ΔE_b the

Table 3
Sample list and results of the temperature PL intensity fits in terms of peak position, pre-exponential factors A_a and A_b (non-radiative over radiative probability ratios) and energy barriers ΔE_a and ΔE_b

Sample	Conversion of MEK (%)	Peak position (nm)	ΔE_a		A_a	ΔE_b		A_b	ϕ_{XRD} (nm)
Sol–gel TiO_2	24	579	76 K	6.6 meV	7.E+00	442 K	38.1 meV	4.E+03	22
TiO_2 HT2	55	558	28 K	2.4 meV	3.E−01	484 K	41.7 meV	2.E+02	3.7
P25 Degussa	89	607	71 K	6.1 meV	4.E+00	625 K	53.9 meV	3.E+03	25
TiO_2 HT1	96	618	3 K	0.3 meV	1.E+07	690 K	59.5 meV	4.E+10	5.6

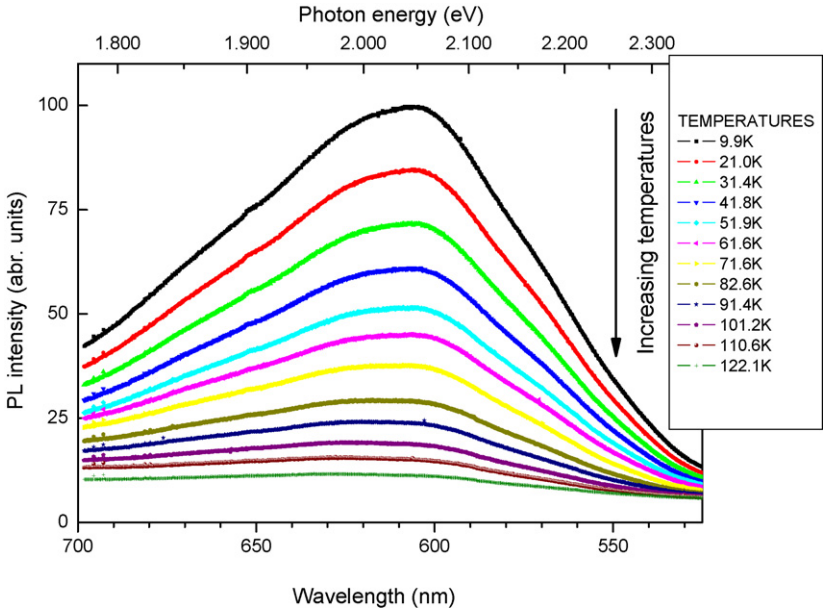

Fig. 4. PL spectra of the P25 TiO_2 (Degussa) sample at different temperatures from 10 up to 122 K.

two energy barriers which are thermally crossed, A_a and A_b are the non-radiative over radiative probability ratios.

Whatever the TiO_2 sample, the use of a two-activation system schematized in Fig. 6, instead of a simple one-level analogue, was necessary to fit the experimental data. Fit results in terms of PL peak position, pre-exponential factors A_a and A_b (non-radiative over radiative probability ratios) and energy barriers ΔE_a and ΔE_b are shown in Table 3.

The first parameter sets (labelled with index 1) explain the low temperatures part of the experimental curves. A very small energy level separation of a few meV, can be easily crossed by the carriers and induce a first partial quenching of the PL. This phenomenon is thus not very efficient, as shown by a probability ratio A_a in the range 1–10, except for the HT1 powder which displays a very high probability ratio. The second activation process acts at higher temperature, as characterized by ΔE_b energies which are larger than 35 meV (400 K). This phenomenon is also more efficient, with a A_b parameter larger than 1000, which reflects the large PL quenching at room-temperature.

Such observations could support the hypothesis of a transfer of the photoexcited carriers to two different surface states at which photogenerated electrons and holes could be trapped. First, it gives rise to a quenching of the light emission, as the carriers are not anymore available for radiative recombination. On the other hand, photogenerated electrons and holes can be used for chemical reactions at the crystallite surface.

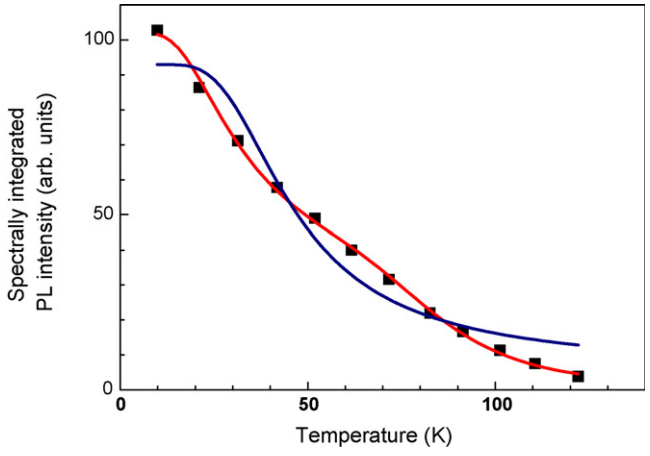

Fig. 5. Spectrally integrated PL intensity (black squares) as a function of the temperature for the P25 TiO_2 (Degussa) sample. The full blue line corresponds to a simple activation law model, while the full red line is the best fit using a double activation law model. (For interpretation of the references to color in this figure legend, the reader is referred to the web version of the article.)

3.3. Discussion

Whatever the crystallite size of the TiO_2 powders, the photocatalysts showed a similar oxygen-to-titanium surface atomic ratio while different contents of OH surface groups were measured. No correlation could be obtained for both parameters

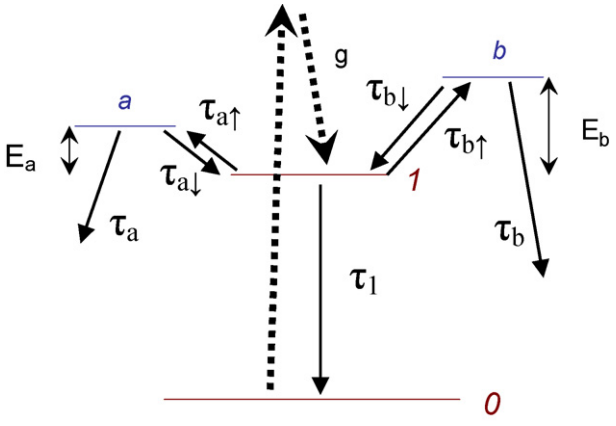

Fig. 6. Scheme of energy state of recombination sites.

with the photocatalytic activity, although the density of surface hydroxyl groups is often reported to positively act on the overall photocatalytic performances [22]. This means that, although the content of OH surface groups is probably beneficial to the activity, it is not the determining factor on the TiO_2 powders used in the present study, and another hypothesis should be put forward to explain the differences in degradation efficiency.

Table 2 shows the adsorption capacities of the TiO_2 samples relatively to MEK (μmol/g) and H_2O (mmol) molecules during the on stream dark-pretreatment period. The obtained values have been corrected from the surface area of TiO_2 available for the reactant adsorption, and thus expressed as μmol/m^2 and mmol/m^2, respectively. Table 3 reports the photocatalytic activity and the temperature photoluminescence properties of titania powders.

It should be pointed out that the MEK removal efficiency could not be directly correlated to the specific surface area, the mean crystallite size and the mean particle size of the TiO_2 photocatalysts. A positive effect on the photocatalytic performances obviously results from the decrease in the crystallite and particle sizes. This leads to the increase in the surface area of the materials and thus in the reactant adsorption capacity for MEK and water molecules, enhancing the pollutant degradation and the $OH^{\bullet}$ radical generation, respectively. However, comparing the MEK and H_2O amounts adsorbed per meter square of available TiO_2 surface for the samples (Table 2) shows that the photocatalytic reaction is not fully controlled by the adsorption step. Indeed, for instance, the HT2 powder displayed a lower MEK adsorption capacity than the sol–gel TiO_2 and the P25 per meter square of available TiO_2 surface. In addition, both HT1 and HT2 nanopowders exhibited totally different performances whereas they displayed a similar H_2O adsorption capacity of 0.07 mmol/m^2.

The powders with the highest photocatalytic activity have a PL peak position around a wavelength of 607–618 nm, whereas the other powders with a lower activity displayed a PL peak at lower values around 558 and 579 nm. Thus, the peak position may be related to the photocatalytic activity. A shift towards shorter wavelengths is usually observed when the particle size decreases due to the modification of electronic properties. Jung et al. have reported that the shift of the peak maximum position to short wavelength means that the energy gap between the lowest exited state and the ground state becomes enlarged [7]. This would be related to changes in the structural irregularity of titania (lattice deformation), thus structural ordering, induced by thermal treatment for example, leads to the shortening of the PL wavelength. However, the method implemented to synthesize the nanoparticles renders such a lattice deformation not realistic and the shift observed is certainly due to another parameters, such as the particle size. Indeed, the HT1 and HT2 nanopowders have been prepared under similar synthesis conditions, and displayed different PL peak positions at 618 and 558 nm, respectively, which is in agreement with a short wavelength shift resulting from the decrease in particle size (5.6 and 3.7 nm, respectively).

The effect of the crystallite size may be compared with HT1 and HT2 nanopowders which have been synthesized under similar hydrothermal conditions, both monodisperse and made of 100% anatase (Figs. 1 and 2) [12,13]. The photocatalytic activity is higher over the nanopowder with the larger grain size, which exhibits very different PL parameters. The PL parameters confirm that the HT1 nanopowder displays the better energetic conditions to limit the photogenerated charge recombination. These results are in agreement with the observation that a too small particle size results in a decrease in the photocatalytic activity due to a higher recombination rate of photogenerated carriers, and confirmed as usual that an optimum in particle size has to be obtained.

However, the position of the PL peak of P25 TiO_2 with an average grain size around 25 nm is located at a wavelength similar to that of HT1 with a smaller average grain size of 5.6 nm. This may be explained by the heterogeneous structure of P25 powder which contains both rutile and anatase crystallographic phases with strong interfaces. The association and coupling of these two semiconductor phases within the P25 TiO_2 is often reported as one of the parameter to explain the high photoactivity of the material [23–25], by allowing a more efficient photogenerated charge separation to be obtained.

Temperature dependent PL results showed that two energy states exist and would allow to hinder the photogenerated charge recombination. As observed before, the first activation process displayed low energy parameters and did not differentiate the different titania samples, except for the non-radiative over radiative probability ratio (A_a) which was very high for the TiO_2 powder which displayed the higher photocatalytic activity. A stronger relationship is observed with the second activation process. Indeed, the energy barrier (ΔE_b) is higher with TiO_2 powders exhibiting the higher photocatalytic activity and with HT1 powder the probability ratio is very high by comparison with the other samples. A strong relationship is thus again observed with these data and the photocatalytic activity.

The photoactivity of the TiO_2 nanoparticles is strongly depending on the temperature, as shown by Anpo et al. by comparing results at liquid nitrogen and at room temperatures [7,9]. The transfer of photoexcited charges (electrons and holes) into surface sites, where they can efficiently catalyse reactions, implies nevertheless that they cross energy gap between states. These processes are thermally activated. At very low temperature, they show a very low probability and the charges disappear mainly by radiative recombination. Transfer process becomes more and more efficient with increasing temperature. This results in a quenching of the light emission. Thus, by recording the photoluminescence intensity as a function of the temperature, we are able to measure the efficiency of the transfer processes. Moreover, comparison with results obtained by Tang et al. [26] over titania bulk crystals shows that trapping processes occur at lower temperatures in our titania nanoparticles. This supports that surface trapping is a dominant mechanism.

4. Conclusion

Measurement of the optical emission properties as a function of the temperature has been developed as a supplementary tool

to get information on the relationship between the photocatalytic activity and the intrinsic properties of the photocatalysts. Well-characterized and calibrated TiO_2 powders including hydrothermally synthesized nanopowders have been used. The thermally activated quenching of the light emission led to record the photoluminescence intensity as a function of the temperature, which allowed the efficiency of the transfer processes to be measured and led thus to determinate their parameters like transfer probability and energy separation between levels. A two-activation model was necessary to fit the temperature PL experimental data, rather than a simple activation law. A relationship/link is observed between the photocatalytic activity and parameters extracted from the temperature PL spectra, such as the peak position and the parameters of the second activation process. The results allowed two different energetic processes to be evidenced and could support the hypothesis of a transfer of the photogenerated carriers to surface states. Time-resolved experiments are currently under investigation.

Acknowledgments

This work was carried out in an "Action Concertée Incitative" framework under the auspices of the French Educational Ministry. P. Bernhardt (LMSPC, UMR 7515 CNRS) and Dr. O. Heintz (LRRS, UMR 5613 CNRS) are thanked for performing XPS analyses. C. Ulhacq (IPCMS, UMR 7504 CNRS), Dr. R. Chassagnon (LRRS) and Prof. C. Esnouf (INSA Lyon) are acknowledged for their assistance in TEM and HRTEM experiments.

Reference

[1] (a) M. Schiavello (Ed.), Photocatalysis and Environment. Trends and Applications, Kluwer academic Publishers, Dordrecht, 1988;
(b) E. Pelizzetti, N. Serpone (Eds.), Photocatalysis. Fundamentals and Applications, Wiley, New York, 1989;
(c) D.F. Ollis, H. Al-Ekabi (Eds.), Photocatalytic Purification and Treatment of Water and Air, Elsevier, Amsterdam, 1993;
(d) J.M. Herrmann, Catal. Today 53 (1999) 115.
[2] N. Serpone, E. Borgarello, M. Grätzel, Chem. Commun. (1984) 32.
[3] (a) Y.C. Liu, G.L. Griffin, S.S. Chan, I.E. Wachs, J. Catal. 94 (1985) 108;
(b) Y.R. Do, W. Lee, K. Dwight, A. Wold, J. Solid State Chem. 108 (1994) 198;
(c) Y.T. Kwon, K.Y. Song, W.I. Lee, G.J. Choi, Y.R. Do, J. Catal. 191 (2000) 192;
(d) A. Di Paola, L. Palmisano, V. Augugliaro, Catal. Today 58 (2000) 141;
(e) C. Martin, G. Solana, V. Rives, G. Marci, L. Palsmisano, A. Sclafani, Catal. Lett. 49 (1997) 235;
(f) P.V. Kamat, B. Patrick, J. Phys. Chem. 96 (1992) 6829;
(g) N. Serpone, P. Maruthamuthu, P. Pichat, E. Pelizzetti, H. Hidaka, J. Photochem. Photobiol. A 85 (1995) 247.
[4] (a) Y. Bessekhouad, D. Robert, J.V. Weber, J. Photochem. Photobiol. A: Chem. 163 (2004) 569;
(b) Y. Bessekhouad, D. Robert, J.V. Weber, Catal. Today 101 (2005) 315.
[5] V. Keller, F. Garin, Catal. Commun. 4 (2003) 377.
[6] (a) M. Anpo, N. Aikawa, Y. Kubokawa, M. Che, C. Louis, E. Giamello, J. Phys. Chem. 89 (1985) 5017;
(b) B. Shelimov, V. Dellarocca, G. Martra, S. Coluccia, M. Che, Catal. Lett. 87 (1-2) (2003) 73.
[7] K.Y. Jung, S.B. Park, M. Anpo, J. Photochem. Photobiol. A: Chem. 170 (2005) 247.
[8] J. Liqiang, F. Honggang, W. Baiqi, W. Dejun, X. Baifu, L. Shudan, S. Jiazhong, Appl. Catal. B: Environ. 62 (2006) 282.
[9] M. Anpo, M. Che, in: W.O. Haag, B.C. Gates, H. Knözinger (Eds.), Advances in Catalysis, vol. 44, 2000.
[10] R. Cleming, The 1994 Information Please Environmental Almanach Complied by World Resources institute, Houghton Mifflin Company, New-York, 1994.
[11] D. Aymes, B. Xin, J.C. Niepce, in: Proceedings of the De la poudre au matériau massif, Albi, France, 2003.
[12] N. Millot, B. Xin, C. Pighini, D. Aymes, J. Eur. Ceram. Soc. 25 (2005) 2013.
[13] C. Pighini, D. Aymes, N. Millot, L. Saviot, J. Nanoparticle Res. 9 (2007) 309.
[14] S. Doniach, M. Sunjic, J. Phys. C: Solid State Phys. 3 (2) (1970) 285.
[15] D.A. Shirley, Phys. Rev. B 5 (12) (1972) 4709.
[16] V. Keller, P. Bernhardt, F. Garin, J. Catal. 215 (2003) 129.
[17] J.T. Mayer, U. Diebold, T.E. Madey, E. Garfunkel, J. Electron Spectrosc. Relat. Phenom. 73 (1995) 1.
[18] J. Guillot, F. Fabreguette, L. Imhoff, O. Heintz, M.C. Marco de Lucas, M. Sacilotti, B. Domenichini, S. Bourgeois, Appl. Surf. Sci. 177 (2001) 268.
[19] D. Zhang, S. Fung, Lin Li-Bin, L. Zhi-Jun, Surf. Coat. Technol. 158-159 (2002) 238.
[20] R. Tanner, Y. Liang, E.I. Altman, Surf. Sci. 506 (3) (2002) 251–271.
[22] Y. Oosawa, M. Grätzel, J. Chem. Soc. Faraday Trans. 1 84 (1988) 197.
[23] T. Kawahara, Y. Konishi, H. Tada, N. Tohge, J. Nishii, S. Ito, Angew. Chem. Int. Ed. 41 (15) (2002) 2811.
[24] B. Sun, P.G. Smirniotis, Catal. Today 88 (2003) 49.
[25] T. Miyagi, M. Kamei, T. Mitsuhashi, T. Ishigaki, A. Yamazaki, Chem. Phys. Lett. 390 (2004) 399.
[26] H. Tang, H. Berger, P.E. Schmid, F. Lévy, G. Burri, Solid State Commun. 87 (1993) 847.